

## BL14B1

### QST Quantum Dynamics II

#### 1. Introduction

BL14B1 is designed for various kinds of diffraction experiments and X-ray absorption fine structure (XAFS)-type spectroscopy measurements in the energy range of 5–90 keV for monochromatized beams and 5–150 keV for white beams. The main optics refers to the standard SPring-8 bending-magnet system with two mirrors and a fixed-exit double-crystal monochromator. These optical elements can be removed completely for an experiment involving white X-rays. This beamline has two experimental hutches. One is dedicated to high-pressure and dispersive XAFS experiments with white X-rays. The other is dedicated to structure analysis of surface and interface, glass, ferroelectrics, catalysts, and metals with monochromatized X-rays. BL14B1 can be a one-stop platform for developments of novel functional materials by complementary use of white and monochromatized X-rays.

#### 2. High-pressure and high-temperature experiments

High-pressure and high-temperature syntheses have been performed at the high-pressure experimental station. *In situ* synchrotron radiation X-ray diffraction measurements can detect structural changes of a sample under high pressure and high temperature. Consequently, the synthetic conditions of novel materials can be easily searched. Additionally, the system can investigate the reaction mechanisms.

Currently, research focuses on synthesizing novel aluminum-based hydrides. In FY2019, novel Al–Ti,

Al–Zr, and Al–Hf hydrides were synthesized. The formed hydrides were recovered at ambient conditions and characterized to clarify their crystal structures and thermodynamic stabilities.

Hydrogenation reactions of pure 3d metals were also investigated. Such reactions occur only at high pressures and cannot be recovered at ambient conditions. Thus, these reactions must be investigated using *in situ* measurement techniques such as synchrotron and neutron diffraction. Previously, our research elucidated the crystal and magnetic structures of double hexagonal close-packed iron deuteride<sup>[1]</sup>, which is a high-pressure phase of iron hydrides. The crystal structure of fcc-NiH<sub>x</sub> was investigated by *in situ* synchrotron and neutron diffraction techniques<sup>[2]</sup>. Here, hydrogenation/deuterization conditions of iron and nickel were carefully investigated using synchrotron radiation X-rays; complementally use of synchrotron and neutron enables us to study hydrogenation/deuterization reactions of metals under high pressure efficiently and quickly. Other metal hydrides have been characterized using this system<sup>[3]</sup>.

#### 3. Stress

In FY2019, a strain scanning measurement employing the energy-dispersive X-ray diffraction method was constructed using the dispersive XAFS (DXAFS) measurement system. Using this system, hydrogen embrittlement in steel materials was investigated from the viewpoint of the stress/strain distribution in materials<sup>[4, 5]</sup>. Based on the obtained residual stress distribution in stretch-formed

tempered martensitic steel specimens together with the finite element method (FEM), it was shown that high residual stress caused cracking on the material when hydrogen was electrochemically charged due to stress-induced hydrogen diffusion [5].

In addition, the double-exposure method with white X-rays (DEM-WX) for the internal stress/strain evaluation of metals with coarse grains was developed using a CdTe area detector [6]. In FY2019, improvement of the diffraction energy accuracy calculated from the Laue spot was evaluated by increasing the distance between the detector and the sample. Although a slight improvement in the accuracy was obtained when the distance increased, further improvements are necessary for strain evaluation.

#### 4. XAFS

XAFS measurements using an energy-dispersive optical system were performed in the white X-ray hutch as well as a conventional optical system in the monochromatic X-ray hutch [7-9]. Various XAFS measurements from high-speed chemical reactions to low-concentration additives can be performed.

Several *in situ* observation conditions can be prepared in the energy-dispersive optics hutch. Remote control systems such as gas flow controllers, switching valves, potentiostats, and injectors are always available. Time-resolved measurements are performed for gas conversion reactions, electrode reactions, ligand substitution reactions, etc. In FY2019, the hydrogenation reaction of Rh nanoparticles was observed by time-resolved XAFS measurements at 50 Hz and the reaction dynamics of dissociatively adsorbed hydrogen atoms were clarified.

In the conventional optics system, low-

concentration XAFS measurements were performed using a 36-element solid-state detector. For example, local structure measurements of Cs-including biotite clay minerals at Cs K-edge XAFS were conducted from the viewpoints of stable storage and volume reduction of radioactive wastes. Observations of a finely milled sample revealed that the layer structure of the biotite clay contributes to the stabilization of the included cesium ions. Research to determine the relationship between the clay structure and the sorption state of cesium ions continues, thereby leading to the mobility evaluation and selective collection of radioactive cesium ions.

#### 5. Diffractometer

Studies of the electrolyte/electrode interfaces were performed using a  $\kappa$ -type multi-axis diffractometer. The surface structure of the Li-ion battery electrode during charge/discharge cycles, the interface structure between solid electrolyte and Pt electrodes, and the electrode surface structure during the electrodeposition reaction in an ionic liquid (IL) were studied. Here, a study on the electrodeposition reaction of Bi in 1-butyl-3-methylimidazolium tetrafluoroborate ([BMIM]BF<sub>4</sub>) on an Au(111) electrode using a surface X-ray scattering (SXS) technique was reported. Previously, it was found that the diffraction peak originated from the surface (1 × 1) structure ((10) peak) and the reflectivity intensity coincided with the cyclic voltammogram. This suggested that the surface structure changes with the electrochemical deposition reaction. However, we examined the surface (1 × 1) structure changes during the electrochemical deposition reaction by continuously measuring the width and the position of the (10) peak during a potential scan.

Neither the position nor the width of the (10) peak changed during the reaction, indicating that the deposited Bi atoms are not alloyed with surface Au atoms, but may form superlattice structures on the Au electrode surface. Although several superlattice structures have been proposed using scanning microscope techniques, the proposed structures were not observed by SXS. Future studies will continue to search for superlattice structures using SXS as well as investigate the dynamics of the electrodeposition reaction of Bi on Au in ILs.

## 6. PDF analysis

$\text{Pb}(\text{Mg}_{1/3}\text{Nb}_{2/3})\text{O}_3$  (PMN) was used in an experiment [10]. The cubic structure of PMN is stable over a wide temperature range. In addition, since a diffuse component can be observed and the PDF amplitude is greatly attenuated, it is suitable as a sample for evaluation. Figure 1 plots  $\chi^2$  and  $R_w$  to evaluate the reliability of the fitting obtained by refining the structural parameters with a cubic structure, which is the average structure, while changing the fitting region every 20 Å. First, by focusing on  $\chi^2$ , the residual error rapidly increased around 50 Å and deviated from the model structure. This is because the local structure differs from the average structure. In addition,  $R_w$  also shows the same tendency because it increased around 50 Å, which is the same as  $\chi^2$ . In particular,  $R_w$  increased slightly in the region of large  $r$  where the PDF amplitude was small. Since this is linked to the decreased PDF amplitude, the results were almost as expected. The box-car refinement showed that  $\chi^2$  and  $R_w$  exhibited the same tendency as an index of reliability of analysis, and the data obtained by BL14B1 satisfied the reliability.

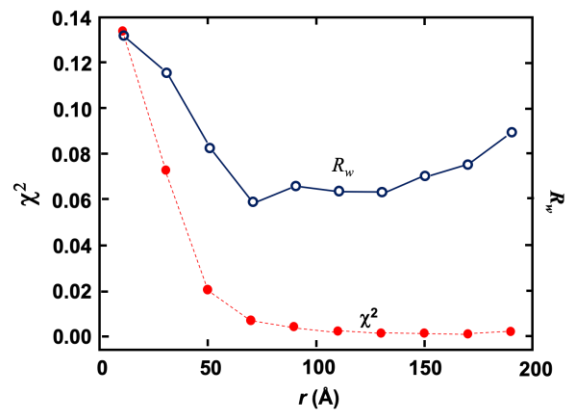


Fig. 1.  $r$  dependence for the agreement factor for PDF analysis,  $\chi^2$  and  $R_w$ .

## 7. X-ray irradiation effects on a tumor

X-ray irradiation effects on a tumor were investigated for Auger therapy. Tumor spheroids containing Gd-loaded nanoparticles were irradiated with synchrotron radiation monochromatic X-rays. The tumor spheroid was completely destroyed using X-rays with  $E = 50.25$  keV, which is just above the Gd K-absorption edge. This indicates that Auger electrons play a key role in the destruction [11, 12].

Hiroyuki Saitoh\*<sup>1</sup>, Ayumi Shiro\*<sup>1</sup>, Ryo Yasuda\*<sup>1</sup>, Takahisa Shobu\*<sup>2</sup>, Yasuhiro Yoneda\*<sup>3</sup>, Kazuhisa Tamura\*<sup>3</sup>, and Daiju Matsumura\*<sup>3</sup>

\*<sup>1</sup> High Pressure Science and Stress Research Group, Synchrotron Radiation Research Center, Kansai Photon Science Institute, Quantum Beam Science Research Directorate, National Institutes for Quantum and Radiological Science and Technology

\*<sup>2</sup> R&D Program Management Department, Japan Atomic Energy Agency

\*<sup>3</sup> Environment and Materials Dynamics Research Group, Materials Sciences Research Center, Japan Atomic Energy Agency

**References:**

- [1] H. Saitoh, A. et al. (2020). *Sci. Rep.*, 10, 9934.
- [2] H. Saitoh, et al. (2020). *Physica B: Condensed Matter*, 587, 412153.
- [3] F. Naoki, et al. (2020). *J. Alloys Compd*, 825, 15830.
- [4] T. Hojo, et al. (2020). *International Journal of Fracture*, 224, 253.
- [5] H. Nishiura, et al. (2020). *ISIJ International Special Issue on Toward Suppression of Hydrogen Absorption and Hydrogen Embrittlement for Steels*, 61, 4.
- [6] K. Suzuki, et al. (2020). *Quantum Beam Science.*, 4, 25.
- [7] Z. Zhang, et al. (2020). *ACS Appl. Mater. Interfaces.*, 12, 6056.
- [8] T. Kobayashi, et al. (2019). *Langmuir.*, 35, 7995.
- [9] D. Matsumura, T. Tsuji, and Kenji. Yoshii. (2019). *Mater. Chem. Phys.*, 238, 121885.
- [10] Y. Yoneda, H. Taniguchi, and Y. Noguchi. (2020). *J. Phys.: Condens. Matter*, 33, 035401.
- [11] K. Matsumoto, etc. (2019) *Scientific Reports*, 9, 13275.
- [12] F. Tamanoi, K. et al. (2020). *Nanomaterials.*, 10, 1341.